International Journal of Architectural Heritage: Conservation, Analysis, and Restoration
Publication details, including instructions for authors and subscription information:
http://www.tandfonline.com/loi/uarc20

A Force-Based Beam FE for the Pushover Analysis of Masonry Buildings

Daniela Addessi [a], Domenico Liberatore [a] & Renato Masiani [a]
[a] Dipartimento di Ingegneria Strutturale e Geotecnica, Sapienza Università di Roma, Via Eudossiana, 18, 00184, Rome, Italy
Accepted author version posted online: 03 Oct 2013.

To cite this article: International Journal of Architectural Heritage (2013): A Force-Based Beam FE for the Pushover Analysis of Masonry Buildings, International Journal of Architectural Heritage: Conservation, Analysis, and Restoration, DOI: 10.1080/15583058.2013.768309

To link to this article: http://dx.doi.org/10.1080/15583058.2013.768309

A Force-Based Beam FE for the Pushover Analysis of Masonry Buildings

Daniela Addessi, Domenico Liberatore and Renato Masiani

Dipartimento di Ingegneria Strutturale e Geotecnica, Sapienza Università di Roma,

Via Eudossiana, 18, 00184 Rome, Italy.

Abstract

A simplified approach for analyzing the nonlinear response of masonry buildings, based on the equivalent frame modeling procedure and on the nonlinear equivalent static analyses, is presented. A nonlinear beam finite element is formulated in the framework of a force-based approach, where the stress fields are expanded along the beam local axis, and introduced in a global displacement-based finite element code. In order to model the nonlinear constitutive response of the masonry material, the lumped hinge approach is adopted and both flexural and shear plastic hinges are located at the two end nodes of the beam. A classical elastic-plastic constitutive relationship describes the nonlinear response of the hinges, the evolution of the plastic variables being governed by the Kuhn-Tucker and consistency conditions. An efficient element state determination procedure is implemented, which condenses the local deformation residual into the global residual vector, thus avoiding to perform the inner loops needed for computing the element nonlinear response. The comparison with some relevant experimental and real full-scale masonry walls is presented, obtaining a very good agreement with the available results, both in terms of global pushover curves and damage distributions.

Keywords: Nonlinear analysis, masonry buildings, force-based FE, equivalent frame, pushover curves.

1 Introduction

The formulation of efficient and accurate numerical models for the structural assessment of masonry buildings is a significant and topical challenge, both related to the preservation of the architectural heritage and historical buildings and to the rational design of new structures. Several approaches have been proposed in literature for modeling masonry structures, with particular reference to the historical buildings. The most sophisticated modeling procedures analyze the masonry structural components by using 2D and 3D finite element (FE) formulations and employing constitutive laws capable to model the complex nonlinear mechanisms characterizing masonry mechanical response, such as damage, cohesion, friction plasticity, crushing, among other aspects. Depending on the scale of detail at which masonry is analyzed, they may be classified into micromechanical models (Gambarotta and Lagomarsino 1997 part i), macroscopic phenomenological models (Gambarotta and Lagomarsino 1997 part ii, Lourenço 1998, Addessi et al. 2002) and multi-scale procedures (Trovalusci and Masiani 2005, Massart et al. 2007, De Bellis and Addessi 2011, Addessi and Sacco 2012, Pau and Trovalusci 2012). The main drawback of such sophisticated models is related to the large modeling and computational requirements and to the need of identifying a large number of material parameters, representing generally a hard task. All these reasons make them not very used for practical purposes. Thus, some of the most refined proposed models, such as the micromechanical and multi-scale

modeling techniques, have been applied up to now to the study of single structural components, such as a single panel.

Other interesting approaches, mainly oriented to design purposes, are the simplified procedures based on the use of 2D macro-elements for modeling each pier and spandrel with a single FE, where a properly constitutive law is defined (Braga and Liberatore 1990). A simplified two degrees of freedom macro-element has been formulated in Gambarotta and Lagomarsino (1996) for describing both the overtuning and the hysteretic shear response of masonry panels under dynamic loading conditions. A generalization of this formulation has been presented in Brencich and Lagomarsino (1998), who proposed a macro-element characterized by eight displacement degrees of freedom, six related to the end nodes and two representing internal variables. In particular, a damage-friction model has been employed and both the overtuning and shear mechanisms have been modeled.

Alternatively, equivalent frame models have been proposed by a number of authors, which have been extensively used for practical analysis of common unreinforced masonry structures (Magenes and Della Fontana 1998, Roca et al. 2005, Penelis 2006, Chen et al. 2008, Belmouden and Lestuzzi 2009, Grande et al. 2011). In particular, for the study of building systems composed of load bearing walls, a frame equivalent model made of beam FEs is adopted, where each wall with opening is decomposed into an assemblage of piers and spandrels, properly connected by means of rigid elements.

Concerning the formulation of the beam FE, the classical displacement-based approach is undoubtedly the more widely used; it assumes compatible displacement and strain fields along

the element, using polynomial interpolation functions, which satisfy the requested continuity conditions. On the other hand, in presence of nonlinear constitutive behavior, where non smooth and localized distributions of deformations in the structural element are expected, a fine and non uniform discretization is needed to satisfactorily describe the mechanical behavior, both in terms of global force-displacement curves and of local stress and strain variations. Moreover, in the case of the Timoshenko beam theory, the displacement-based FEs are affected by the well-known shear locking problems. Starting from an alternative point of view, in various works (Spacone et al. 1996, Petrangeli and Ciampi 1997, Neuenhofer and Filippou 1998, Taylor et al. 2003, Addessi and Ciampi 2006) it has been demonstrated that beam elements are more suitably defined by adopting a force-based (FB) formulation, which directly interpolates the stress fields along the element. Such approach, although it requires a more complex procedure for the element state determination, is easily introduced in a global displacement-based formulation (Addessi and Ciampi 2006) and results computationally more efficient, especially in presence of constitutive nonlinearity; this implies also the possibility of using coarse meshes for the structural discretization. In fact, since the FB elements assume exact interpolating polynomials for the stress fields, the numerical solution is only affected by the error related to the adopted approximated integration rule, while it is quite independent on the discretization. Based on similar considerations, a variational consistent mixed formulation for a shear deformable beam element, derived from the Hu-Washizu principle, has been proposed by Taylor et al. (2003).

In this paper, a new beam finite element for the analysis of the nonlinear response of masonry buildings, modeled on the basis of the equivalent frame approach, is proposed. As demonstrated in the literature (Magenes 2006), linear elastic analyses, both static and dynamic, are not capable

to satisfactorily reproduce the structural response of masonry buildings. Although the most accurate methodology should be based on the nonlinear dynamic analysis, it is worthwhile noting that it requires very high computational costs and the identification of the mechanical parameters governing the cyclic constitutive laws, which often is very hard and uncertain. In many cases a static nonlinear analysis can realistically describe the main aspects of the global and local responses of the buildings, better than a linear dynamic one.

Concerning the pushover analysis, in Galasco et al. (2004) an effective procedure has been adopted for transforming the problem of pushing a structure, maintaining constant ratios between the applied forces, into an equivalent incremental static analysis with one degree of freedom displacement response control. Subsequently, in Galasco et al. (2006) a new displacement-based algorithm for the adaptive pushover analysis of masonry structures has been proposed, where the load pattern is derived, step-by-step, by the actual deformed shape evaluated during the pushover analysis. Moreover, Anthoine (2006) presented a simple displacement control method able to follow the monotonic pushover curves also along the softening branches, based on an appropriate definition of the displacement variable to be used for controlling the loading process.

In this paper, the static nonlinear analysis methodology is employed. In particular, a FB formulation is adopted, characterized by numerical efficiency and convergence properties better than the classical displacement-based formulation (Spacone et al. 1996, Addessi and Ciampi 2006) and allowing to avoid the shear locking problems. In order to describe the onset of plasticity mechanisms and localized crack bands in critical regions of the masonry, a 2-node FE with lumped plastic hinges located at the ends is adopted, which, although less accurate than a

model with a spread nonlinear constitutive behavior, allows to capture the relevant aspects of the nonlinear masonry structural response with a very low computational burden. Therefore, such simple FE formulation enables to satisfactorily describe also the static nonlinear response of the masonry under loading conditions simulating seismic actions, resulting at the same time very efficient from the computational point of view and easy to be used by designers. The beam FE, formulated on the basis of the Timoshenko theory under the hypothesis of small displacements and deformations, consists of a central element, whose constitutive behavior is linear elastic, and two hinges arranged in series at the ends, characterized by a nonlinear constitutive law both regarding the bending and the shear behavior. The Italian seismic code (NTC 2008) is employed for determining the yielding moments of the flexural hinges and the yielding force of the shear hinge, as well as the displacement ultimate thresholds. As concerns the computational aspects, a nonlinear solution algorithm based on a consistent element state determination procedure and on a predictor-corrector hinge state determination method is adopted. The proposed force-based element is implemented in the FE code FEAP (Taylor 2011). In Section 2, the FB formulation of the beam FE with end lumped hinges is presented and the constitutive relationships, adopted for modeling the nonlinear response of the flexural and shear hinges, are introduced; in Section 3 the solution algorithm is illustrated; finally, in Section 4 two numerical applications on full-scale masonry structures are presented, by comparing the numerical results obtained by using the proposed FE with the experimental ones and with the results numerically evaluated by adopting different FE models.

2 Beam finite element formulation

The formulation of the 2D beam element, here used, assumes Timoshenko theory and geometrically linear behavior. The element forces and displacements are expressed in the local reference system by the following vectors (Fig. 1(b)):

$$\mathbf{Q} = \{Q_1 Q_2 Q_3\}^T ; \ \mathbf{q} = \{q_1 q_2 q_3\}^T \tag{1}$$

where Q_1 and Q_2 are the bending moments at the end nodes 1 and 2, and Q_3 is the axial force. Similarly, q_1 and q_2 are the nodal deformational rotations and q_3 is the axial elongation. Both **Q** and **q** are related to the six component vectors **P** and **p** (Fig. 1(a)), containing the nodal forces and displacements expressed in the global reference system, by applying the operators **R**, which projects **P** and **p** in the local reference system, and **B**, which eliminates the displacement components defining the rigid modes. The following relations hold:

$$\mathbf{q} = \mathbf{BRp} ; \ \mathbf{P} = \mathbf{R}^T \mathbf{B}^T \mathbf{Q} \tag{2}$$

where:

$$\mathbf{R} = \begin{bmatrix} \cos\alpha & \sin\alpha & 0 & 0 & 0 & 0 \\ -\sin\alpha & \cos\alpha & 0 & 0 & 0 & 0 \\ 0 & 0 & 1 & 0 & 0 & 0 \\ 0 & 0 & 0 & \cos\alpha & \sin\alpha & 0 \\ 0 & 0 & 0 & -\sin\alpha & \cos\alpha & 0 \\ 0 & 0 & 0 & 0 & 0 & 1 \end{bmatrix} ; \quad \mathbf{B} = \begin{bmatrix} 0 & 1/L & 1 & 0 & -1/L & 0 \\ 0 & 1/L & 0 & 0 & -1/L & 1 \\ -1 & 0 & 0 & 1 & 0 & 0 \end{bmatrix}$$

being α the angle between the local and global axes, x and X, and L denoting the element length (Fig. 1(a)). The section stress and deformation vectors are defined as:

$$\mathbf{S}(x)=\{N(x)\ T(x)\ M(x)\}^T;\ \mathbf{d}(x)=\{\varepsilon(x)\ \delta(x)\ \chi(x)\}^T \quad (3)$$

where $N(x)$ is the axial force, $T(x)$ the shear force and $M(x)$ the bending moment, while $\varepsilon(x)$ is the axial deformation along the reference axis x, $\delta(x)$ the shear deformation and $\chi(x)$ the curvature.

Since the beam FE is composed of a series of three elements, for the definition of the relations governing equilibrium inside the element, and only regarding the bending components, it is necessary to distinguish between the moments at the end nodes of the central element, indicated with Q_{1e} and Q_{2e}, and the ones defined at the hinges, indicated with Q_{1h} and Q_{2h}. Obviously, a similar subdivision is not necessary for the axial force component Q_3, since the plastic hinges are defined only for the flexural and shear behavior. Therefore, the following equilibrium relations hold:

$$Q_i = Q_{ie} = Q_{ih} \quad (4)$$

with i=1, 2.

As regards the central element, the force-based formulation, here adopted, is based on the polynomial interpolation of the element section stress field:

$$\mathbf{S}(x_e)=\mathbf{b}(x_e)\mathbf{Q}_e=\mathbf{b}(x_e)\mathbf{Q} \quad (5)$$

where the vector $\mathbf{Q}_e$ collects the stress components Q_{1e}, Q_{2e} and Q_3 and the equilibrium matrix $\mathbf{b}(x_e)$ is expressed as:

$$\mathbf{b}(x_e)=\begin{bmatrix} 0 & 0 & 1 \\ 1/L_e & 1/L_e & 0 \\ x_e/L_e-1 & x_e/L_e & 0 \end{bmatrix}$$

being L_e the length of the central element and x_e the local axial coordinate with the origin located at the first node of the central element. When distributed loads along the element are neglected, constant axial and shear forces and linear variation of the bending moment along the element describe exactly the stress fields in the element, which satisfy equilibrium.

Similarly, for deriving the relationships governing the kinematic, it is necessary to define the rotational degrees of freedom at the end nodes of the inner element and the rotations of the plastic hinges. The first are denoted with q_{ie}, the second with q_{ih}. As a result of series arrangement of the element and hinges, the following relation can be written:

$$q_i = q_{ie} + q_{ih} \quad (6)$$

Furthermore, since at each end i both a bending and shear plastic hinge is located, the rotation q_{ih} is expressed as the sum of two contributions as:

$$q_{ih} = q_{ihb} + q_{ihs} \quad (7)$$

where q_{ihb} represents the rotation of the bending hinges, while q_{ihs} is the rotational contribution of the shear plastic hinges. The displacement degrees of freedom at the end nodes of the central

element, $\mathbf{q}_e = \{q_{1e}\, q_{2e}\, q_3\}^T$, can be evaluated on the basis of the section deformations $\mathbf{d}(x_e)$, by exploiting the following integral relation:

$$\mathbf{q}_e = \int_0^{L_e} \mathbf{b}(x_e)^T \mathbf{d}(x_e)\, dx_e \qquad (8)$$

Vectors $\mathbf{S}(x_e)$ and $\mathbf{d}(x_e)$ are related by means of a generalized constitutive law, which may involve the section stiffness matrix $\mathbf{k}_s(x_e)$, or, in a force-based approach, the section flexibility matrix $\mathbf{f}_s(x_e)$, relating the increment of the deformation vector, $\dot{\mathbf{d}}(x_e)$, to the increment of the stress vector, $\dot{\mathbf{S}}(x_e)$. In the case of isotropic linear elastic behavior and constant geometrical and mechanical cross-section parameters along the beam axis x_e, it results:

$$\mathbf{f}_s = \begin{bmatrix} \frac{1}{EA} & 0 & 0 \\ 0 & \frac{1}{GA^*} & 0 \\ 0 & 0 & \frac{1}{EI} \end{bmatrix}$$

where E and G are the Young's modulus and the shear elasticity modulus, respectively, and A, A^*, I are the area, shear area and moment of inertia of the beam cross-section. By applying the principle of the virtual work, the relation between the nodal displacement degrees of freedom $\mathbf{q}_e$ and the nodal forces $\mathbf{Q}_e$ is derived in the form:

$$\mathbf{q}_e = \mathbf{F}_e\, \mathbf{Q}_e \qquad (9)$$

being governed by the element flexibility matrix $\mathbf{F}_e$, defined as:

$$\mathbf{F}_e = \int_0^L \mathbf{b}(x_e)^T \mathbf{f}_s \, \mathbf{b}(x_e) \, dx_e = \begin{bmatrix} \frac{L_e}{3EI} + \frac{1}{L_e GA^*} & -\frac{L_e}{6EI} + \frac{1}{L_e GA^*} & 0 \\ -\frac{L_e}{6EI} + \frac{1}{L_e GA^*} & \frac{L_e}{3EI} + \frac{1}{L_e GA^*} & 0 \\ 0 & 0 & \frac{L_e}{EA} \end{bmatrix} \quad (10)$$

As concerns the plastic hinge constitutive behavior, an elastic-plastic law is adopted and the incremental constitutive relationships may be written for the flexural hinges in the form:

$$\dot{q}_{ihb} = F_{ihb} \, \dot{Q}_i \quad (11)$$

and for the shear hinges as:

$$\dot{q}_{ihs} \, l_c = F_{ihs} \frac{\dot{Q}_1 + \dot{Q}_2}{L_e} \quad (12)$$

Since a constant interpolation has been adopted for the shear component along the element, a single shear plastic hinge can be considered. Note that, in order to determine the shear deformation governing the constitutive response of the shear hinge, the increment of the rotation in Eq. 12 is multiplied by a length parameter l_c associated to the hinge. The quantities F_{ihb} and F_{ihs}= F_{hs} are the tangent flexibility coefficients of the flexural and shear hinges, respectively. By introducing the constitutive relationships Eqs. 9, 11 and 12 into the kinematic Eqs. 6, 7 and 8, the flexibility matrix of the element composed by the series of the central elastic element and the end plastic hinges is determined as:

$$\mathbf{F}=\begin{bmatrix} \frac{L_e}{3EI}+\frac{1}{L_eGA^*}+F_{1hb}+\frac{F_{hs}}{l_c L_e} & -\frac{L_e}{6EI}+\frac{1}{L_eGA^*}+\frac{F_{hs}}{l_c L_e} & 0 \\ -\frac{L_e}{6EI}+\frac{1}{L_eGA^*}+\frac{F_{hs}}{l_c L_e} & \frac{L_e}{3EI}+\frac{1}{L_eGA^*}+F_{2hb}+\frac{F_{hs}}{l_c L_e} & 0 \\ 0 & 0 & \frac{L_e}{EA} \end{bmatrix} \quad (13)$$

Since the global solution procedure is based on the displacement method, matrix **F** has to be inverted to obtain the stiffness matrix **K** and the element internal forces **Q** have to be determined.

2.1 Plastic hinges constitutive behavior

2.1.1 Flexural hinges

An elastic-plastic constitutive model with kinematic hardening is adopted for both the flexural and shear hinges. In particular, in the case of the flexural hinges, the moment-rotation relationship is written in incremental form as:

$$\dot{M}_i = K_{ihb}\left(\dot{q}_{ihb}-\dot{q}_{ip}\right) \quad (14)$$

where M_i is the moment at the flexural hinges located at the first (i=1) and last (i=2) node of the FE, respectively, evaluated by solving the elastic-plastic constitutive relations; q_{ip} is the plastic rotation of the hinge; K_{ihb} is the tangent elastic-plastic stiffness coefficient. The evolution law of the plastic rotation is expressed for the hinge at node i as:

$$\dot{q}_{ip} = \dot{\lambda}_{ib} \frac{\partial F_{ib}}{\partial M_i}$$
$$F_{ib} \le 0 \quad ; \quad \dot{\lambda}_{ib} \ge 0 \quad ; \quad F_{ib}\dot{\lambda}_{ib} = 0$$
$$\dot{F}_{ib}\dot{\lambda}_{ib} = 0 \qquad (15)$$

where the second and third rows of Eqs. 15 contain the Kuhn-Tucker loading-unloading conditions and the consistency condition, respectively. In particular, λ_{ib} represents the inelastic multiplier and F_{ib} is the plastic loading-unloading limit function, which is expressed as:

$$F_{ib} = |M_i - \gamma_i| - M_{yi} \qquad (16)$$

with M_{yi} denoting the yield moment and γ_i representing the kinematic hardening variable, whose evolution is governed by:

$$\dot{\gamma}_i = H_i \, \dot{q}_{ip} \qquad (17)$$

being H_i the kinematic hardening coefficient.

Aiming to employ the proposed beam FE for the seismic analysis of masonry buildings modeled as equivalent frames, where each wall with opening is decomposed into an assemblage of piers and spandrels properly connected by means of rigid elements, the evaluation of the ultimate moment M_{yi} can be made according to standard seismic codes. In particular, in this paper the Italian seismic code (NTC 2008) is employed and the adopted formulae are reported in Appendix A.

2.1.2 Shear hinge

The incremental constitutive law of the shear hinge is expressed in terms of the shear deformation, s, and the shear force, T, as:

$$\dot{T} = K_{hs}\left(\dot{s} - \dot{s}_p\right) \qquad (18)$$

with s_p denoting the plastic shear deformation and K_{hs} the tangent stiffness coefficient. Similarly to the flexural hinges, the evolution process of the plastic variable s_p is governed by the Kuhn-Tucker inequalities and by the consistency condition, which appear as:

$$\begin{aligned} &\dot{s}_p = \dot{\lambda}_s \frac{\partial F_s}{\partial T} \\ F_s \le 0 \quad ; \quad &\dot{\lambda}_s \ge 0 \quad ; \quad F_s \dot{\lambda}_s = 0 \\ &\dot{F}_s \dot{\lambda}_s = 0 \end{aligned} \qquad (19)$$

where λ_s is the inelastic multiplier and the plastic limit function F_s is defined similarly to the case of the flexural hinges, that is:

$$F_s = \left|T - \gamma\right| - T_y \qquad (20)$$

The evolution of the kinematic hardening variable γ is governed by:

$$\dot{\gamma} = H\,\dot{s}_p \qquad (21)$$

with H denoting the kinematic hardening coefficient. Concerning the evaluation of the shear yield threshold T_y, the Italian seismic code is followed (see Appendix A).

2.2 Rigid offsets introduction

When the equivalent frame modeling procedure is used for describing the seismic response of masonry walls, subdivided into piers and spandrels modeled as beam FEs, it is required to properly reproduce the regions of the masonry walls where piers and spandrels interact. To this end, rigid offsets are introduced in the FE formulation. In particular, the presence of rigid offsets parallel and orthogonal to the element axis *x* are considered, as illustrated in Fig. 2. By denoting with $\overline{\mathbf{P}}$ the nodal force vector at the end nodes of the rigid offsets, the following relation is derived:

$$\overline{\mathbf{P}} = \mathbf{B}_R \, \mathbf{P} \qquad (22)$$

with:

$$\mathbf{B}_R = \begin{bmatrix} \mathbf{B}_{R1} & \mathbf{0} \\ \mathbf{0} & \mathbf{B}_{R2} \end{bmatrix}$$

where:

$$\mathbf{B}_{R1} = \begin{bmatrix} 1 & 0 & 0 \\ 0 & 1 & 0 \\ -\left(l_{x1}\sin\alpha + l_{y1}\cos\alpha\right) & \left(l_{x1}\cos\alpha - l_{y1}\sin\alpha\right) & 1 \end{bmatrix}$$

and

$$\mathbf{B}_{R2} = \begin{bmatrix} 1 & 0 & 0 \\ 0 & 1 & 0 \\ \left(l_{x2}\sin\alpha + l_{y2}\cos\alpha\right) & -\left(l_{x2}\cos\alpha - l_{y2}\sin\alpha\right) & 1 \end{bmatrix}$$

and **0** denotes the 3x3 null matrix; l_{xi} and l_{yi} represent the rigid offset lengths at the end i of the FE, parallel and orthogonal to the beam axis, respectively.

By exploiting the virtual work equivalence, the transformation rule for the nodal displacement degrees of freedom is deduced as:

$$\mathbf{p} = \mathbf{B}_R^{\,T}\,\bar{\mathbf{p}} \qquad (23)$$

3 Solution algorithm

The numerical solution of the global incremental non-linear equilibrium equations, governing the response of the 2D frame model, follows a classical step-by-step method for the time integration and a standard iterative Newton-Raphson algorithm. The FB formulated FE and the developed solution algorithm are implemented in the general-purpose FE analysis program FEAP (Taylor 2011), which is used to perform all the numerical analyses. The assembling procedure of the global stiffness matrix and of the residual vector is performed by FEAP, which requires, at the element level, the computation of the element stiffness matrix $\bar{\mathbf{K}} = \mathbf{B}_R\,\mathbf{K}\,\mathbf{B}_R^{\,T}$ and the structural reaction force vector $\bar{\mathbf{P}}$. The methodology developed for the element state determination is schematically illustrated in Table 1. Note that, in the case of the presented FB approach, the element state determination procedure is more complex than for the classical displacement-based

formulation and it is presented in some detail, following a procedure similar to the ones proposed in Petrangeli and Ciampi (1997), Neuenhofer and Filippou (1998), Addessi and Ciampi (2006).

In the following, 'Δ' denotes the increment of the quantities in the time step Δt and the superscript 'k' the value of the variables at the current Newton-Raphson iteration. After evaluating the current increment of the element forces $\Delta\mathbf{Q}^k$ on the basis of the increment of the element displacements $\Delta\mathbf{q}^k$ and the element flexibility matrix at the previous iteration $\mathbf{F}^{k-1}$, the current increment of the rotations, Δq_{ihb}^k, and shear deformation, Δs^k, for the flexural and shear hinges, respectively, are evaluated. Then, the flexural hinge rotations, q_{ihb}^k, and the shear hinge deformation, Δs^k, are updated and the constitutive relationships are solved. Therefore, the new hinge flexibilities, F_{ihh}^k and F_{hs}^k, and the hinge moments and shear, M_i^k and T^k, are calculated. On the basis of the current hinge flexibility coefficients and the flexibility matrix of the central element, $\mathbf{F}_e$, the current flexibility matrix of the overall element, $\mathbf{F}^k$, is updated and, finally, by its inversion, the new element stiffness $\mathbf{K}^k$ is computed. As for the element structural reaction forces $\mathbf{Q}^k$, the deformation residuals at the hinges, ρ_{ihb}^k and ρ_{hs}^k, are first determined, based on the difference between the equilibrated forces $\left(\mathbf{Q}^{k-1}+\Delta\mathbf{Q}^k\right)$ and the values obtained by the constitutive laws, M_i^k and T^k. Such hinge deformation residuals are transformed into the element deformation residual, $\mathbf{r}^k$, by summing the contributions of the flexural and shear hinges at each node. By pre-multiplying $\mathbf{r}^k$ by the element stiffness $\mathbf{K}^k$, a residual on the element structural reaction forces is calculated, which is used to compute the updated $\mathbf{Q}^k$. Finally, in order to take into account the presence of the rigid offsets and the rotation from the local

reference system to the global one, the transformations in Eqs. 2 and 22 are performed. Both the updated $\overline{\mathbf{K}}^k$ and $\overline{\mathbf{P}}^k$ are passed to the global code FEAP for the assembling and solution procedures; as the Newton-Raphson global iterations go on, also the local deformation residual $\mathbf{r}^k$ tends to reduce to zero and the global iteration loops at each time step are repeated until a norm of the solution is less than some tolerance. In particular, an energy convergence test is performed at the global level, according to the classical methodology implemented in FEAP, and the inner product of the global displacement vector and the global residual vector at the current iteration, normalized with respect to the corresponding value at the first iteration, is compared with an energy tolerance, here assumed equal to 1E-9. Note that, since a consistent element state determination procedure is adopted, at the element level no iterations are needed and the computed element deformation residual, $\mathbf{r}^k$, is condensed into the residual on the element structural reaction forces and passed back at the global level. The solution of the elastic-plastic constitutive law for the hinges follows a predictor-corrector technique.

4 Numerical Applications

In the following, two examples are presented concerning an experimental prototype and a real full-scale masonry building and the numerical results are compared with the experimental ones and with other numerical FE models.

4.1 Pavia's test

The first example concerns the analysis of a two-storey unreinforced masonry wall, which is a part of a full-scale building prototype, tested at the Pavia University. In this application the door wall D (Fig. 3(a)), which has been extensively studied in literature (Gambarotta and Lagomarsino 1997 part ii, Magenes and Della Fontana 1998, Grande et al. 2011), is analyzed. Two uniformly distributed vertical loads, whose values are p_1=14.1 *kN*/*m* and p_2=13.8 *kN*/*m*, respectively, are applied at the floor levels. Then, the structural model is subjected to increasing lateral forces, which are applied at the floor levels, keeping a 1:1 ratio between the forces at the first and second floor. The mechanical parameters adopted for the piers and the spandrels are selected in line with the Italian seismic code (NTC 2008), referring to the values prescribed for a good masonry, and are reported in Table 2. The wall thickness is equal to 0.25 *m*. The piers and the spandrels are modeled by the proposed beam FE, assuming for the cross-section dimensions the wall thickness and the pier length or the wall thickness and the spandrel height, respectively. In order to reproduce the rigid plane constraint due to the presence of stiff steel beams at each floor, the horizontal displacements of the nodes at the floors are linked to be equal. The FE model adopted for performing the numerical analyses is shown in Fig. 3(b), where the rigid offsets defined in each FE are indicated by the thick lines, whose length has been evaluated by exploiting the formula proposed by Dolce (1991) for the piers and considering the clear length as the flexible region of the spandrels. The parameter l_c associated to the shear hinge is assumed equal to 0.01L, being L the FE length. The distributed vertical loads p_1 and p_2 are applied at the floor nodes as concentrated vertical forces. As concerns the lateral horizontal forces, F, they are

applied with a 1:1 ratio at the floor levels, by means of a system of stiff trusses and beams. A horizontal displacement is applied to the node where the two stiff beams are connected (Fig. 3(b)), allowing to transfer two equal forces at the floor levels and to perform a displacement-controlled analysis.

In Fig. 4 the global response curve is reported, by depicting the total base shear versus the horizontal displacement measured at the second floor. On the top horizontal axis the drift values are reported, corresponding to the second floor displacement values reported on the bottom horizontal axis. The curve numerically obtained by using the beam FE presented above (solid line) is compared with the experimental one (triangle symbols) (Gambarotta and Lagomarsino 1997 part ii) and with the curve evaluated by applying the multi-scale procedure proposed in De Bellis and Addessi (2011) (dashed line) and by adopting the material parameters reported in Gambarotta and Lagomarsino (1997 part ii). The results computed by means of the simplified frame model show satisfactory agreement with both the experimental curve and the numerical one, evaluated by using a 2D FE discretization. It is worthwhile noting that, although the dashed line curve, obtained by means of the multi-scale procedure, matches better the experimental results with respect to the curve evaluated with the proposed equivalent frame model (solid line), the computational costs of the multi-scale procedure are much higher. Moreover, the final value of the total base shear force for the two numerical models are less than 5% different.

In Fig. 5 the distributions of the plastic hinges at three different loading steps are reported: Fig. 5(a) corresponds to the top displacement u=3 *mm* and to the drift δu=0.053%, Fig. 5(b) to u=4 *mm* and δu =0.070% and Fig. 5(c) to u=12 *mm* and δu =0.208%. The flexural hinge at the base of

the left pier and the two shear hinges in the spandrels at the first floor develop for $u<3$ *mm*; after that also the flexural hinge at the top of the left pier at the second floor appears ($u=3$ *mm*). The final distribution shows flexural hinges at the base and at the top of the left piers, at the base of the other two at the first floor and at the top at the second floor, as well as shear hinges in all the spandrels. The collapse load equal to 137 *kN* is attained, when the flexural hinges appear at the base of the three piers, and a difference of 10%, compared to the experimentally obtained value, is observed. The final step of the analysis corresponds to the formation of the local mechanism at the first floor characterized by the presence of the flexural hinges at the base of the three piers (Fig. 5(c)), then causing the numerical loss of convergence.

Also the distribution of the flexural and shear hinges matches very well the experimental distribution of the damage and micro-fractures, as well as the ones obtained by means of much more sophisticated FE modeling approaches (Gambarotta and Lagomarsino 1997 part ii). In Fig. 6 the distribution of the displacement at the two floors is reported at the three loading steps (a), (b) and (c), where a more pronounced interstorey drift is shown at the first floor. In Figs. 7 and 8 the values of the axial and shear stresses, respectively, at the base of the three piers is shown at the same loading steps. The left and right piers undergo the minimum and maximum value of the axial stress, respectively, due to their location with respect to the horizontal imposed displacement. Since the flexural and shear strengths of the piers both depend on the axial force (see Appendix A), it results that the damaging mechanisms appear in the left pier before than in the middle and right ones, as it can be observed in Fig. 5. Instead, in Fig. 8 it is shown that shear stress values are higher in the middle pier due to its higher length, while the lowest values appear

in the left one. Note that, as the applied horizontal displacement increases, the axial and shear stress values decrease in the left piers and increase in the right one.

4.2 Old masonry building

The second example concerns an old masonry building located in Catania (Italy), Via Martoglio, analyzed by various researchers in the framework of The Catania Project (Liberatore 2000). In particular, the inner wall made of regular blocks shown in Fig. 9 is studied. It is five storey made of clay brick masonry and supported by reinforced concrete ring beams. The roof is supported by a timber structure. All the floors have a thickness of 0.30 *m*, while the last floor thickness is 0.16 *m*. The analyzed wall is geometrically regular, except for the large opening at the center of the first floor. The wall is modeled by adopting the proposed FE for the piers and the spandrels connected by rigid offsets and by introducing standard linear elastic beam FEs for modeling the reinforced concrete ring beams located at the floors, with a cross section of dimensions 0.30x0.24 m^2. The adopted frame discretization is shown in Fig. 10, where the rigid offsets defined in each FE are indicated by the thick lines. The mechanical parameters adopted for the piers and the spandrels, derived on the basis of available experimental results and of previous numerical analyses on similar buildings in the framework of The Catania Project and adopted by all the research groups involved (Liberatore 2000) for analyzing the 'Via Martoglio' building, are reported in Table 2. The parameter l_c is assumed equal to $0.01L$, being L the FE length. In Table 3 the values of the total vertical loads applied at each floor are reported. In the last row the distribution of the seismic horizontal loads is also shown, where F_{hj} denotes the lateral seismic force at the level j and F_{htot} the total base shear. As in the previous example, a displacement-

controlled nonlinear static analysis is performed and the horizontal seismic loads are applied by means of a system of stiff trusses and beams, connected to the masonry wall equivalent frame at the floor levels (Fig. 10).

In Fig. 11 the global response curves are reported, i.e. the total base shear versus the top displacement measured at the last floor. The results obtained by adopting the proposed FE (continuous curve without symbols) are compared with the ones presented in Liberatore (2000) and obtained with different numerical models. In particular, the curves with the diamond and triangle symbols, reported by Magenes and Braggio in Liberatore (2000), refer to the equivalent frame FE model proposed by Magenes and Della Fontana (1998). In such model, only the shear mechanisms are taken into account for the spandrels; furthermore, the curve with triangles is obtained by considering for the piers only the formation of flexural hinges, while the curve with diamonds refers to the possible formation in the piers of shear hinges. Finally, the curve with cross symbols, reported by Liberatore and Spera in Liberatore (2000), is referred to a different modeling approach, based on the so-called macro-elements and considering a no-tension constitutive law for the masonry (Braga and Liberatore 1990). It can be observed that the curve computed with the proposed FE (continuous curve) approaches very closely the one with diamond symbols, but a little lower ultimate load is obtained, equal to 1170 *kN*. It has to be noted that the model here presented allows the formation of both flexural and shear hinges in both the piers and the spandrels, thus resulting more severe than the modeling assumptions on which the results by Magenes and Braggio are based. In Figs. 12 (a) and (b) the distribution of the hinges in the frame is reported at two steps, referring to the top displacement and drift values u=0.011 *m* and δu =0.056% (a), u=0.014 *m* and δu =0.072% (b), respectively. After the initial linear elastic

behavior, flexural hinges appear in some piers located at the last floor and shear hinges in the spandrels at the first and second floor (Fig. 12 (a)). The formation of the hinges proceeds rapidly and the collapse load is reached when flexural hinges appear at the base of all the piers located at the last floor (Fig. 12 (b)), thus causing the formation of a local mechanism. As a consequence, the loss of convergence at the final step stops the analysis. Therefore, such results confirm the ones also obtained by Liberatore and Spera in Liberatore (2000) that the last floor is a weak part of the wall, due to the low values of the applied vertical loads and to the absence of the reinforced concrete ring beams. Finally, in Fig. 13 the displacement distribution along the height of the wall is reported at the two steps (a) and (b), where it appears that the interstorey drift is more pronounced at the first three floors.

5 Conclusions

An equivalent frame model for the analysis of the nonlinear in-plane response of masonry walls under lateral forces, simulating the seismic actions, has been presented. In particular, an equilibrium-based FE formulation has been proposed for the beam elements modeling the masonry piers and spandrels. The lumped hinge approach has been adopted in order to model the nonlinear constitutive response of the masonry, introducing at the end sections of the beam elements both flexural and shear plastic hinges. The numerical applications performed on both an experimental masonry wall and on an old real masonry building have showed that the proposed simplified modeling procedure is able to satisfactorily reproduce the global pushover response curves and the distribution of the damage in the walls, although with a very low computational burden. The adoption of the force-based formulation for the beam FE has allowed to avoid the

shear locking problems, affecting the classical displacement-based Timoshenko beam FEs, and simultaneously to obtain an efficient numerical procedure, characterized by very good convergence properties.

As for the numerical algorithm implemented for solving the element state determination problem at each loading time step, the adopted consistent iteration scheme has allowed to further reduce the computational costs, avoiding to perform the local iterative loops needed to determine the nonlinear response at the element level.

Thus, the proposed model may be usefully employed for design purpose, representing an efficient and robust tool for evaluating the pushover response curves of the masonry walls with low computational costs. Furthermore, it may be easily extended to the 3D analysis of masonry building under seismic loads. Further developments will allow the adoption of a cyclic constitutive relationship for the flexural and shear lumped hinges, taking into account the progressive damaging mechanisms affecting the strength and stiffness mechanical properties of the masonry and making it possible to perform nonlinear dynamic analyses under the seismic cyclic loading conditions.

Appendix A

The evaluation of the flexural strength of the piers, i.e. the ultimate moments M_{yi} calculated at the end sections of the piers, can be made according to the Italian seismic standard code, assuming an equivalent stress-block diagram for masonry in compression. In the following the subscript '*i*' is neglected. For rectangular sections it results:

$$M_y = \frac{1}{2} l^2 t \sigma_0 \left(1 - \frac{\sigma_0}{0.85 f_c}\right) \quad (24)$$

where l and t are the pier length and thickness, respectively, σ_0 is the mean vertical stress equal to $N/(lt)$ and f_c is the masonry compressive strength.

The ultimate displacement is assumed equal to 0.8% of the height of the panel.

As concerns the spandrels, the following expression is adopted for the ultimate moment:

$$M_y = \frac{H_p h}{2} \left(1 - \frac{H_p}{0.85 f_h h t}\right) \quad (25)$$

with H_p the minimum value between the tensile strength of the horizontal element in tension (ring beams or chains) and $0.4 f_h h t$, being f_h the masonry compressive strength along the horizontal direction and h the height of the spandrel cross section.

The shear strength of the piers, calculated according to the Italian seismic code, results:

$$T_y = l' t f_v \quad (26)$$

where l' is the length of the compressed zone in the panel end sections and f_v is the masonry shear strength evaluated as:

$$f_v = f_{v0} + 0.4 \sigma_n \leq f_{vLIM} \quad (27)$$

being f_{v0} the masonry mean shear strength and σ_n the mean vertical stress acting on the compressed zone of the panel. The value of f_v is bounded by the shear strength limit value f_{vLIM}. The ultimate displacement is assumed equal to 0.4% of the height of the panel.

In the case of old masonry, characterized by irregular fabric or weak blocks, the shear strength can be computed, for example, by means of the Turnsek-Cacovic formula (Turnsek and Cacovic 1970) and it results:

$$T_y = lt\frac{f_t}{b}\sqrt{1+\frac{\sigma_0}{f_t}} \quad (28)$$

where f_t is the tensile strength for diagonal cracking and b is defined as:

$$b = \frac{h}{l} \quad 1 \le b \le 1.5 \quad (29)$$

As for the spandrels, the ultimate value of the shear is computed as:

$$T_y = h\,t\,f_{v0} \quad (30)$$

References

Addessi, D., Marfia, S., and Sacco, E. 2002. A plastic nonlocal damage model. Comput. Method. Appl. M., 191:1291-1310.

Addessi, D., and Sacco, E. 2012. A multi-scale enriched model for the analysis of masonry panels. Int. J. Solids Struct., 49(6): 865-880.

Addessi, D., and Ciampi, V. 2006. A regularized force-based beam element with a damage-plastic section constitutive law. Int. J. Numer. Meth. Eng., 123:958-966.

Anthoine, A. 2006. A simple displacement control technique for pushover analyses. Earthquake Engng Struct. Dyn., 35:851–866.

Belmouden, Y., and Lestuzzi, P. 2009. An equivalent frame model for seismic analysis of masonry and reinforced concrete buildings. Constr. Build. Mater., 23(1):40-53.

Braga, F., and Liberatore, D. 1990. A finite element for the analysis of the response of masonry buildings under seismic actions. In Proc. of the 5th North American Masonry Conference, Urbana, USA.

Brencich, A., and Lagomarsino, S. 1998. A macro-elements dynamic model for masonry shear walls. In Proc. STRUMAS IV—4th Int. Symp. on Computer Methods in Structural Masonry, E&FN Spon, London :67–75.

Chen, S.-Y., Moon, F.L., and Yi, T. 2008. A macroelement for the nonlinear analysis of in-plane unreinforced masonry piers. Eng. Struct., 30(8):2242-2252.

De Bellis, M.L., and Addessi, D. 2011. A Cosserat based multi-scale model for masonry structures. Int. J. Multiscale Com., 9(5):543-563.

Dolce, M. 1991. Schematizzazione e modellazione degli edifici in muratura soggetti ad azioni sismiche (Modelling of masonry buildings under seismic loads). L'Industria delle Costruzioni, 242:44-57, (in Italian).

Galasco, A., Lagomarsino, S., Penna, A., and Resemini S. 2004. Non-linear seismic analysis of masonry structures. Proc. of 13th World Conference on Earthquake Engineering, Vancouver.

Galasco, A., Lagomarsino, S., and Penna A. 2006. On the use of pushover analysis for existing masonry buildings. Proc. of First European Conference on Earthquake Engineering and Seismology, Geneva.

Gambarotta, L., and Lagomarsino, S. 1996. On the dynamic response of masonry panels. In Proc. of the National Conference "Masonry Mechanics Between Theory and Practice", Messina, Italy (in Italian).

Gambarotta, L., and Lagomarsino S. 1997. Damage models for the seismic response of brick masonry shear walls part i: the mortar joint model and its application. Earthquake Eng. Struc. D., 26:423-439.

Gambarotta, L., and Lagomarsino S. 1997. Damage models for the seismic response of brick masonry shear walls part ii: the continuum model and its application. Earthquake Eng. Struc. D., 26:441-462.

Grande, E., Imbimbo, M., and Sacco, E. 2011. A beam finite element for nonlinear analysis of masonry elements with or without fiber-reinforced plastic (FRP) reinforcements. Int. J. Archit. Herit., 5:693-716.

Liberatore, D., 2000. Progetto Catania: Indagine sulla risposta sismica di due edifici in muratura (The Catania Project: Investigation on the seismic response of two masonry buildings). GNDT National Group for Seismic Protection: Rome, (in Italian).

Lourenço, P. B. 1998. Continuum model for masonry: parameter estimation and validation. J. Sruct. Eng., 124(6):642-652.

Magenes, G., and Della Fontana, A. 1998. Simplified linear seismic analysis of masonry buildings. Proc. Br. Masonry Soc., 8:190-195.

Magenes, G. 2006. Masonry building design in seismic areas: recent experiences and prospects from a European standpoint. Keynote 9, In Proc. of the 1st European Conference on Earthquake Engineering and Engineering Seismology, Geneva, Switzerland.

Massart, T. J., Peerlings, R. H. J., and Geers, M. G. D. 2007. An enhanced multi-scale approach for masonry wall computations with localization of damage. Int. J. Numer. Meth. Eng., 69:1022-1059.

M.I.T., 2008. D.M. 14.01.2008. Norme Tecniche per le Costruzioni, Ministero Infrastrutture e Trasporti: Rome, Italy (in Italian).

Neuenhofer, A., and Filippou, F.C. 1998. Geometrically nonlinear flexibility-based frame finite element. J. Sruct. Eng., 124:704-711.

Pau, A., and Trovalusci, P. 2012. Block masonry as equivalent micropolar continua: the role of relative rotations, Acta Mechanica, 223(7):1455-1471.

Penelis, G.G. 2006. An efficient approach for pushover analysis of unreinforced masonry (URM) structures. J. Earthquake Eng., 10(3):359-379.

Petrangeli, M., and Ciampi, V. 1997. Equilibrium based iterative solutions for the non-linear beam problem. Int. J. Numer. Meth. Eng., 40:423-437.

Roca, P., Molins, C., and Marì, A.R. 2005. Strength capacity of masonry wall structures by the equivalent frame method. J. Sruct. Eng., 131(10):1601-1611.

Spacone, E., Ciampi, V., and Filippou, F.C. 1996. Mixed formulation of nonlinear beam finite element. Comput. Struct., 58 :71-83.

Taylor, R.L., Filippou F.C,. Saritas, A., and Auricchio, F. 2003. A mixed finite element method for beam and frame problems. Comput. Mech., 31:192-203.

Taylor, R., 2011. FEAP - a finite element analysis program, Version 8.3. Department 1233 of Civil and Environmental Engineering, University of California at Berkeley, 1234 California.

Trovalusci, P., and Masiani, R. 2005. A multifield model for blocky materials based on multiscale description. Int. J. Solids Struct., 42: 5778-5794.

Turnsek, V., and Cacovic, F., 1970. Some experimental results on the strength of brick masonry walls. In Proc. of the 2nd International Brick Masonry Conference, 149- 156, Stoke on Trent, UK.

List of figures

Fig. 1: Beam FE: nodal displacements (bottom) and forces (top) in the global (a) and local (b) reference system.

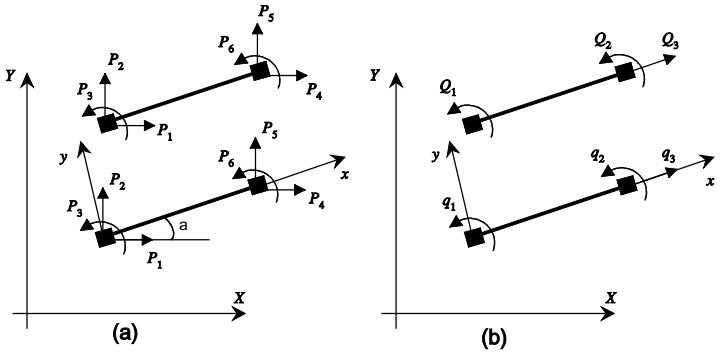

Fig. 2: FE with rigid offsets.

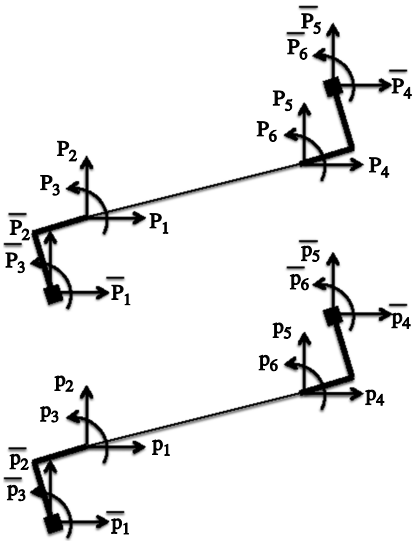

Fig. 3: Pavia's test: structural model (a); FE model (b).

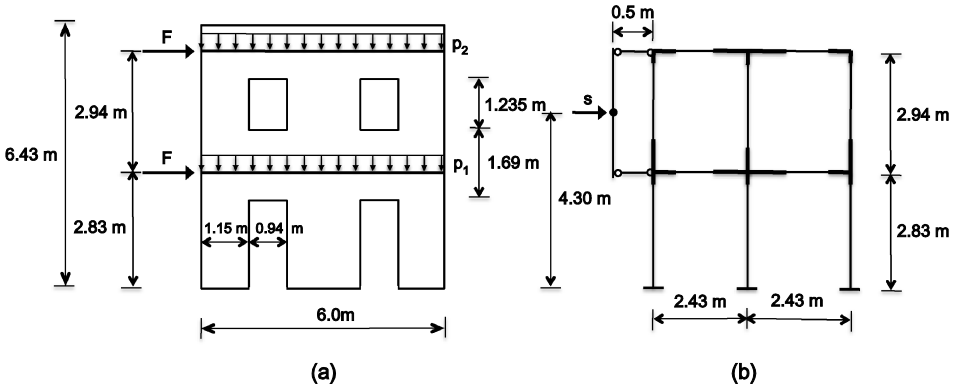

Fig. 4: Pavia's test: global response curves.

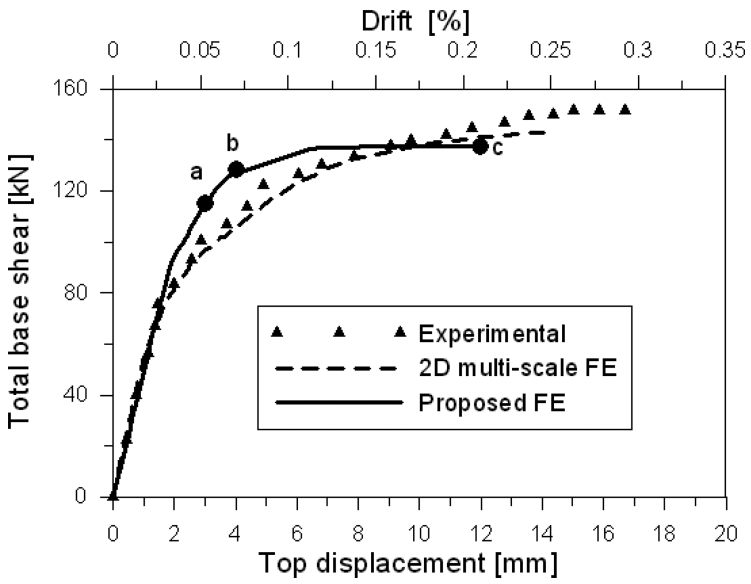

Fig. 5: Pavia's test: distribution of the plastic hinges at the three loading steps reported in Fig. 4, *u*=3 *mm*, *u*=4 *mm*, *u*=12 *mm*.

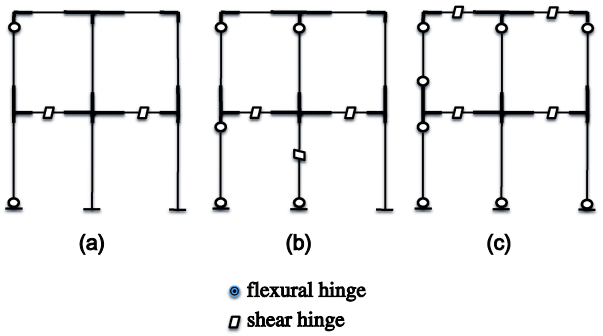

Fig. 6: Pavia's test: floor displacement distribution at the three loading steps reported in Fig. 4, u=3 *mm*, u=4 *mm*, u=12 *mm*.

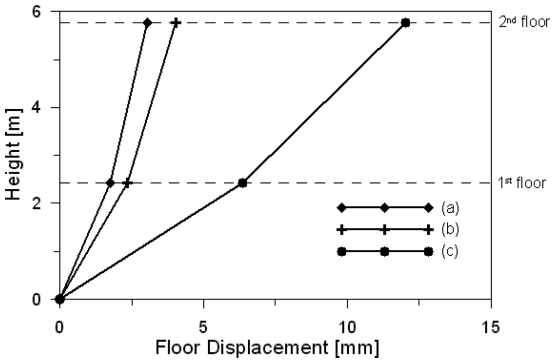

Fig. 7: Pavia's test: axial stresses at the base of the piers at the three loading steps reported in Fig. 4, *u*=3 *mm*, *u*=4 *mm*, *u*=12 *mm*.

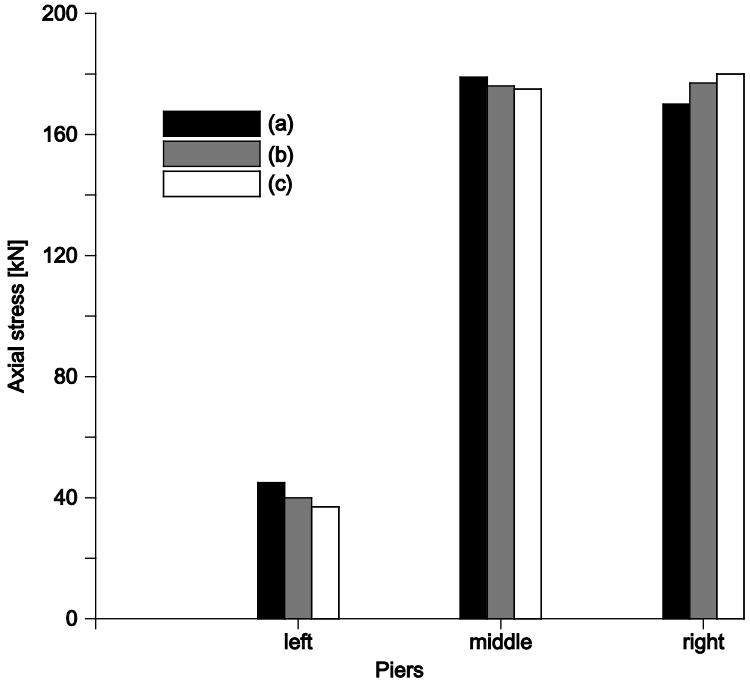

Fig. 8: Pavia's test: shear stresses at the base of the piers at the three loading steps reported in Fig. 4, u=3 *mm*, u=4 *mm*, u=12 *mm*.

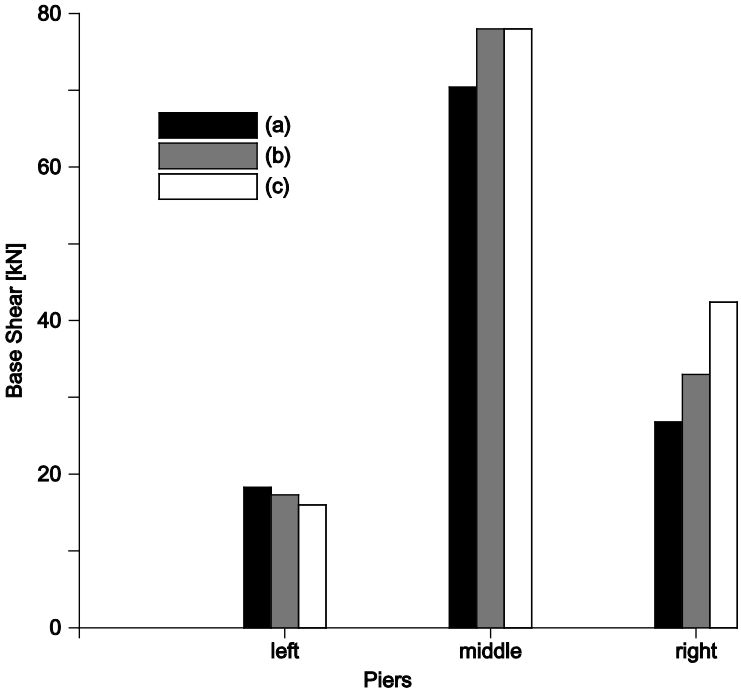

Fig. 9: Via Martoglio masonry wall: structural model.

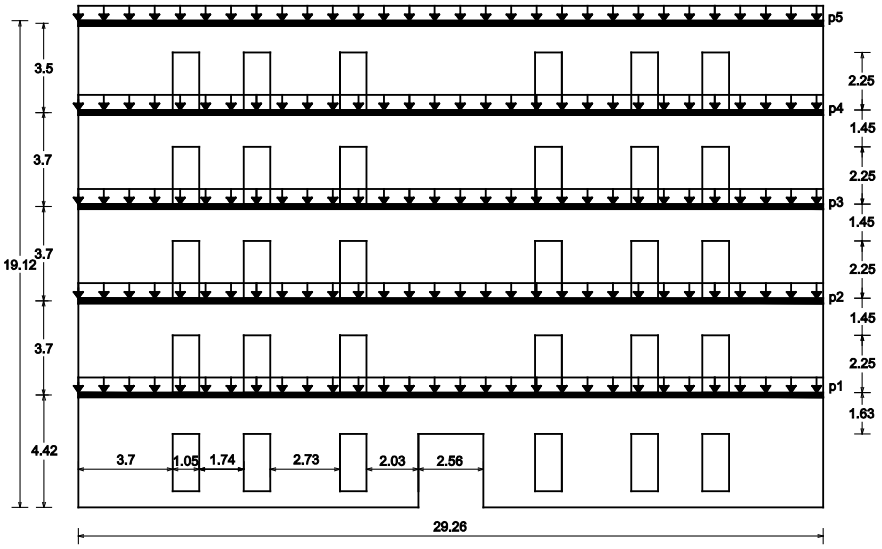

Fig. 10: Via Martoglio masonry wall: FE model.

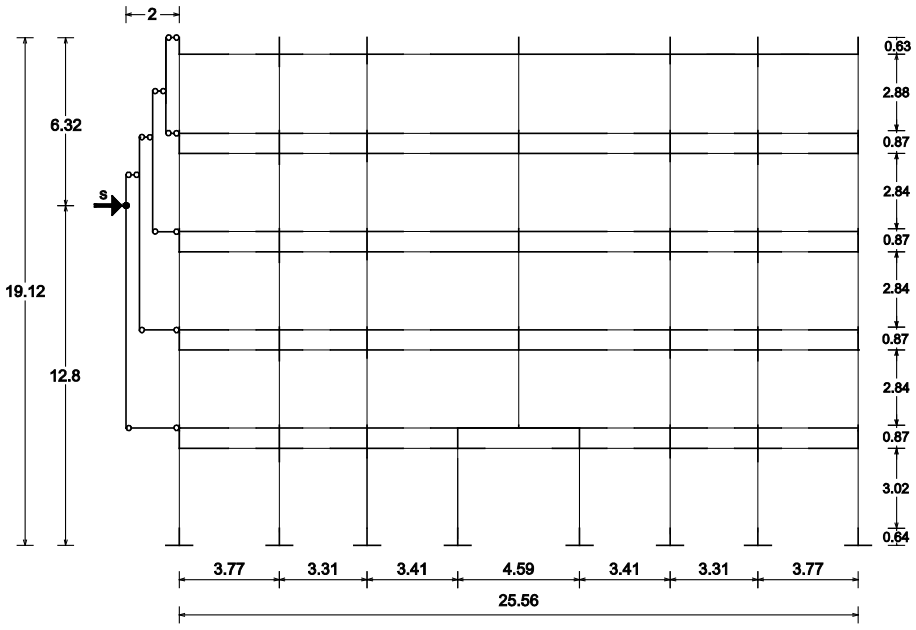

Fig. 11: Via Martoglio masonry wall: global response curves.

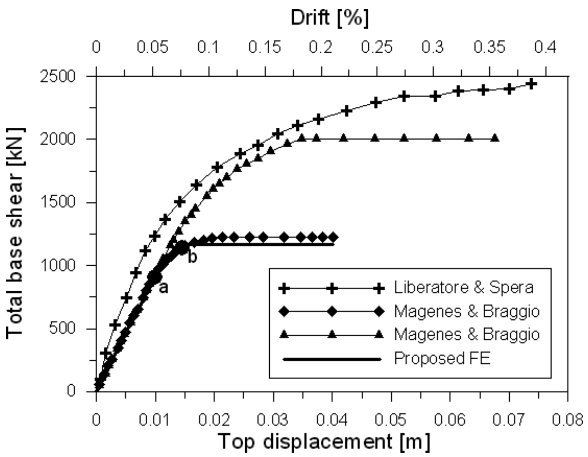

Fig. 12: Via Martoglio masonry wall: distribution of the plastic hinges at the steps (a) and (b) reported in Fig.11, *u*=0.011 *m, u*=0.014 *m*.

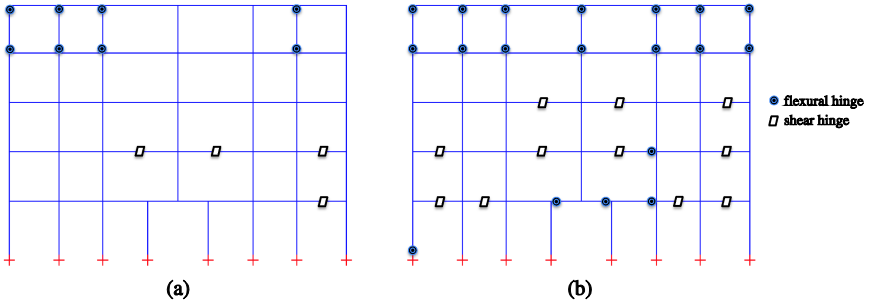

Fig. 13: Via Martoglio masonry wall: floor displacement distribution at the two steps reported in Fig.11, *u*=0.011 *m, u*=0.014 *m*.

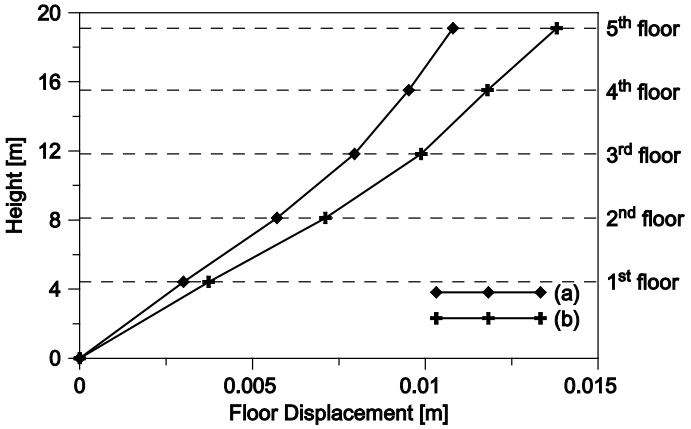

List of tables

ACCEPTED MANUSCRIPT

Table 1: Element state determination procedure at the iteration '*k*'.

$\Delta\mathbf{p}^k$	global displacement increment
$\Delta\mathbf{q}^k = \mathbf{B}\mathbf{R}\Delta\mathbf{p}^k$	local displacement increment
$\Delta\mathbf{Q}^k = \left(\mathbf{F}^{k-1}\right)^{-1}\Delta\mathbf{q}^k$	local nodal force increment
$\Delta q_{ihb}^k = F_{ihb}^{k-1}\Delta Q_i^k \quad ; \quad \Delta s^k = F_{hs}^{k-1}\frac{\Delta Q_1^k + \Delta Q_2^k}{L_e}$	deformation increments at the hinges
$M_i^k, T^k \quad ; \quad F_{ihb}^k, F_{hs}^k$	solution of the constitutive relationships of the hinges
$\mathbf{F}^k$	current element flexibility matrix
$\rho_{ihb}^k = F_{ihb}^k\left(Q_i^{k-1} + \Delta Q_i^k - M_i^k\right)$	rotational residual at the flexural hinge *i*

$\rho_{hs}^{k} = \frac{F_{hs}^{k}}{l_c}\left(\frac{Q_1^{k-1} + Q_2^{k-1}}{L_e} + \frac{\Delta Q_1^{k} + \Delta Q_2^{k}}{L_e} - T^{k}\right)$	rotational residual at the shear hinge
$\mathbf{r}^{k} = \left\{\rho_{1hb}^{k} + \rho_{hs}^{k} \quad \rho_{2hb}^{k} + \rho_{hs}^{k} \quad 0\right\}^{T}$	vector of the nodal displacement residual
$\mathbf{Q}^{k} = \mathbf{Q}^{k-1} + \Delta\mathbf{Q}^{k} - \left(\mathbf{F}^{k}\right)^{-1}\mathbf{r}^{k}$	updated element nodal force vector
$\overline{\mathbf{K}}^{k} = \mathbf{B}_{R}\,\mathbf{R}^{T}\,\mathbf{B}^{T}\left(\mathbf{F}^{k}\right)^{-1}\mathbf{B}\mathbf{R}\mathbf{B}_{R}^{T}$	updated element stiffness matrix
$\overline{\mathbf{P}}^{k} = \mathbf{B}_{R}\,\mathbf{R}^{T}\,\mathbf{B}^{T}\mathbf{Q}^{k}$	updated global nodal force vector

Table 2: Mechanical parameters.

Pavia's test					
E (kN/m^2)	G (kN/m^2)				
1.8E6	0.6E6				
f_c (kN/m^2)	f_t (kN/m^2)	f_h (kN/m^2)	f_{v0} (kN/m^2)	H_p (kN/m^2)	f_{vLIM} (kN/m^2)
2800	96.6	1400	64.4	204	2200
Via Martoglio masonry wall					
E (kN/m^2)	G (kN/m^2)				
1.6E6	0.3E6				
f_c (kN/m^2)	f_t (kN/m^2)	f_h (kN/m^2)	f_{v0} (kN/m^2)	H_p (kN/m^2)	f_{vLIM} (kN/m^2)
6000	225	3000	150	97.18	2200

Table 3: Via Martoglio masonry wall: applied load values.

Floor level	1	2, 3	4	5
Masonry dead load (*kN*)	504	470	365	128
Floor load (*kN*)	286	353	345	53
Total load (*kN*)	790	823	710	181
Seismic load F_{hj}/F_{htot}	0.101	0.194, 0.283	0.320	0.101